Comparative analysis of stimulated Brillouin scattering at 2 μm in various infrared glass-based optical fibers

Moïse Deroh, J.C. Beugnot, Kamal Hammani, Christophe Finot, Julien Fatome, F Smektala, Hervé Maillotte, Thibaut Sylvestre, Bertrand Kibler

Comparative analysis of stimulated Brillouin scattering at 2-µm in various infrared glass-based optical fibers

M. DEROH,[1,2*] J-C. BEUGNOT,[2] K. HAMMANI,[1] C. FINOT,[1] J. FATOME,[1] F. SMEKTALA,[1] H. MAILLOTTE,[2] T. SYLVESTRE,[2] AND B. KIBLER[1]

[1]*Laboratoire Interdisciplinaire Carnot de Bourgogne, UMR 6303 CNRS- Université Bourgogne Franche-Comté, Dijon, France*

[2]*Institut FEMTO-ST, UMR 6174 CNRS-Université Bourgogne Franche-Comté, Besançon, France*

** moise.deroh@femto-st.fr*

Abstract: We provide experimental characterization of stimulated Brillouin scattering at 2-µm wavelength in step-index optical fibers made of various types of infrared materials. Our results show that the main characteristics of the Brillouin process such as the frequency shift, spectral linewidth and gain can be widely tuned through the index-controlled guiding of both acoustic and optical waves as well as the intrinsic material properties of the fiber under test. More precisely, we found that depending on the used material the Brillouin frequency shift can be decreased by 30% in a common step-index fiber design, while its linewidth and gain efficiency can be increased by a factor 5 and 180, respectively, when compared with the standard silica fiber. Four families of fiber materials were analyzed near 2 µm as well as at 1.55 µm for comparison, namely, germanosilicate, zirconium fluoride, tellurium oxide, and sulfur-based chalcogenide. Our findings open the way for further fundamental investigations of stimulated Brillouin scattering and the development of practical applications in the 2-µm spectral range.

1. Introduction

In recent years, the 2-µm spectral window has been extensively exploited in order to design and develop devices and components for several applications such as high-resolution molecular sensing, frequency conversion, imaging, and bio-photonics, lasers and telecommunication systems [1–7]. Such developments have mainly benefited from the emergence of thulium-doped fiber amplifiers (TDFA) that can amplify a broad spectral range around 2 µm. However, to date, most of optical devices such as electro-optic modulators, fibers couplers and lasers sources operating in the 2-µm waveband still need large improvements compared to those existing in the traditional 1.55-µm telecom band. The coherence properties of the continuous-wave (CW) lasers could for instance be enhanced by means of a suitable use of nonlinear effects such as stimulated Brillouin scattering (SBS) [8,9]. SBS is one of the most efficient nonlinear effects in optical materials that arises from the interaction between the optical field and *acoustic* phonons through electrostriction, giving rise to inelastic scattering with a down-frequency shift of a few GHz [8]. Due to its large optical gain and high coherence properties, SBS is now extensively used in a wide range of photonic applications including ultra-low noise narrow-linewidth fiber lasers, distributed fiber sensing, and microwave photonics [10–16]. It is worth to mention however that most of the SBS spectral characterizations and Brillouin fiber lasers (BFL) remain focused on the 1.55-µm wavelength range based on various optical-fiber materials such as silica [9,17], bismuth [18,19], tellurite [20–22], and chalcogenide glasses [23–25]. A large improvement of the Brillouin efficiency using the latter glasses has been reported [26–28]. For instance, Abedin has demonstrated a Brillouin gain coefficient at

1.55 µm in a chalcogenide glass fiber (As_2Se_3) g_B of 6.0×10^{-9} $m.W^{-1}$, about 134 times larger than that of fused silica fiber. Including the effective mode area A_{eff} of the fiber, this actually provides an effective gain efficiency (g_B/A_{eff}) about 513 times larger than in standard silica fibers [23] (153.8 $W^{-1}.m^{-1}$ versus 0.3 $W^{-1}.m^{-1}$). Note that, in the following, we use this suitable parameter (g_B/A_{eff}) that directly characterizes SBS for a given power in optical fibers or waveguides. This gain efficiency can be still increased by tapering a fiber, thus allowing to reach up to 1503 $W^{-1}.m^{-1}$ due to the strong light confinement capability in the resulting small fiber core [29]. More recently, Deroh et *al*. have also unveiled a large SBS efficiency in heavily GeO_2-doped core silica fibers [30]. By contrast, only few works have been reported in the 2-µm waveband. As an example, Luo et *al*. firstly developed a single-frequency Brillouin laser cavity operating at 2-µm, in which three pump diodes with a total power of 18 W were required to overcome a high Brillouin lasing threshold of 1.04 W [31]. Later, the lasing threshold has been greatly reduced down to 52 mW thanks to a specifically designed chalcogenide-glass ($As_{38}Se_{62}$) suspended-core optical fiber [32]. In the same way, distinct Brillouin laser arrangements based on a segment of heavily germanium-doped silica fiber or tellurite-glass fiber have recently been demonstrated with low values of SBS threshold [33,34]. Finally, efficient Brillouin lasing operation around 2-µm can also be obtained with the single-mode silica fiber specifically designed for infrared by Nufern (SM-1950) [35].

In this work, we characterize various types of infrared-glass step-index fibers ranging from standard silica to chalcogenide materials for SBS applications in the 2-µm waveband. We also present additional measurements obtained at 1.55 µm for a suitable comparison and assessment of the impact of pumping wavelength. More specifically, we investigate four families of fiber glasses that can be easily encountered in the literature of step-index fibers dedicated to the high-demand 1.5-3 µm spectral region, namely, germanosilicate, zirconium fluoride, tellurite, and sulfur-based chalcogenide. We find that the most efficient fibers in terms of SBS gain efficiency at 2 µm are the tellurite and chalcogenide fibers with an enhancement factor up to 52 and 180, respectively, compared to the standard SMF-28. We further show that the main features of the SBS, such as the frequency shift, the spectral linewidth and gain can be widely impacted by the index-controlled guiding properties of such a fiber design as well as intrinsic material characteristics.

This work is organized as follows. We first describe the experimental setup and the method used for spectral characterization of SBS. Next, we present in detail our results obtained at 2 µm for the different fibers under test. Then, we compare all the reported data so as to establish a general overview of the SBS efficiency in infrared-glass step-index fibers and discuss the key physical relations and current limitations of such optical fibers. Finally, we conclude and provide some future prospects of this work.

2. Experimental setup

Figure 1 shows the experimental setup used for spectral characterization of SBS. The pump laser consists of a tunable narrow-linewidth (100 kHz) continuous-wave diode laser operating around 2-µm (Thorlabs TLK-L1950R). The laser is first split into two beams by means of a 70:30 fiber coupler (FC). One beam is sent to a thulium-doped fiber amplifier (TDFA) and serves as input pump in the fiber under test (FUT) through an optical circulator (OC), while the other beam is used as a reference beam or local oscillator (LO) for SBS heterodyne detection [36]. The Brillouin signal backscattered from the FUT is then mixed with the reference beam using another 50:50 coupler, thus generating a beat signal, which is further detected with an ultrafast 2-µm photodiode (PD, Newport, 818-BB-51AF). Note that a fiber polarization controller (PC) is also inserted to maximize the resulting beat signal. The Brillouin gain spectrum is finally recorded using an electrical spectrum analyzer (ESA) with a resolution bandwidth of a few kHz. A power-meter is also used in the experimental setup in order to

accurately monitor the fiber transmission during measurements. The optical circulator, polarization controller, and fiber couplers are all made of single-mode silica fiber dedicated to the 2-µm spectral band and characterized by low losses.

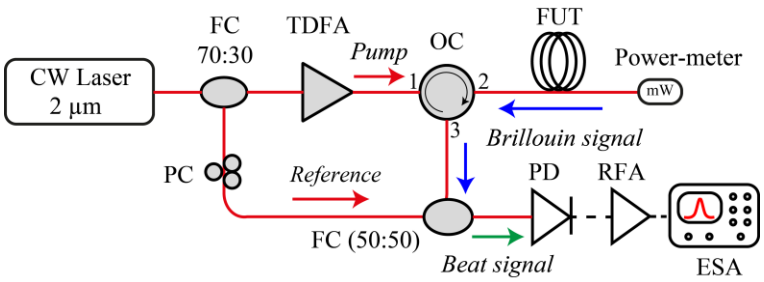

Fig. 1. Experimental setup of the heterodyne detection technique for measuring the Brillouin frequency shift and spectral linewidth in FUT. CW: continuous wave, FC: fiber coupler, TDFA: thulium-doped fiber amplifier, OC: optical circulator, FUT: fiber under test, PD: photodiode, RFA: radiofrequency amplifier, ESA: electrical spectrum analyzer.

3. Germania-doped-core silica fibers

We first study the dependence of Brillouin scattering properties in five distinct single-mode germanosilicate core fibers as a function of GeO_2 content and related guiding properties (see also Table 1 in section 6). More specifically, we used a standard single-mode fiber (3.6% mol, SMF-28, black line), a standard highly nonlinear fiber (HNLF) from Sumitomo Electrics (21% mol, HNLF, blue line) and three heavily doped-core fibers from the Fiber Optic Research Center (FORC, Russia) with increasing doping levels: 53% mol (red line), 75% mol (green line), and 98% mol (purple line), respectively. Note that all the Brillouin spectra were measured in the spontaneous regime well below the Brillouin threshold. As can be clearly seen in Fig. 2(a), the Brillouin frequency shift (BFS) strongly reduces from 8.39 GHz down to 6 GHz when increasing the GeO_2 content in the fiber core. The BFS evolves in a quadratic manner as a function of the doping level. The corresponding Brillouin linewidth, shown in Fig. 2(b), is found to significantly increase up to 76 MHz with respect to the GeO_2 core concentration. It is worth to highlight that the BFS and spectral linewidth values measured at 2 µm in all the fiber samples are lower than those reported in the case of a 1.55-µm pump wavelength [30]. This will be discussed in more details in section 6. Moreover, we notice in Ref. [35], that SMF-28 and SM-1950 fused silica fibers do not exactly manifest the same BFS and spectral linewidth, which can be related to their slightly distinct guiding properties (i.e., index profile and core diameter).

The SBS gain coefficient g_B can be straightforwardly estimated from the Brillouin linewidth (see Eq. 2 in section 6) [8,36]. We then calculated the Brillouin gain efficiency g_B/A_{eff} ($W^{-1}.m^{-1}$) for all our germanosilicate fibers (see inset in Fig. 2(a)). It clearly appears that the SBS gain efficiency increases almost linearly with the GeO_2 doping level. For instance, for 98-mol % it is about 6 times larger than in the standard silica fiber. Indeed, the GeO_2 doping level strongly changes the elastic properties such as the elastic phonon velocity, young modulus and the mass density (for more details, see Table 1 in section 6). Correspondingly, the longitudinal acoustic velocity strongly decreases when increasing the core doping level. Concerning the optical wave, the effective refractive index also increases with GeO_2 content, while the effective mode area (from 101 μm^2 for SMF-28 down to 5 μm^2 for 98-mol % at 2 µm) strongly reduces to satisfy the single-mode operation driven by the index profile of the fiber. As a consequence, such fibers give rise to both large nonlinear Kerr coefficients and Brillouin efficiency at such

wavelengths. However, when only considering the SBS gain coefficient g_B intrinsically related to the fiber core material, this value is decreasing with GeO_2 doping level.

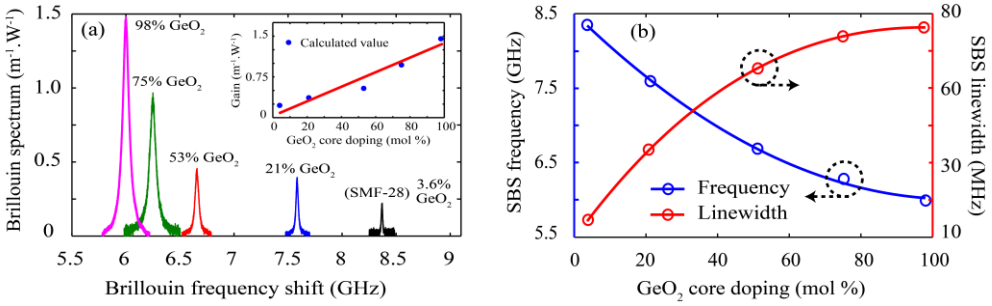

Fig. 2. (a) Experimental Brillouin spectra measured at 2-µm in five distinct GeO_2-doped core fibers from low (3.6 mol %) up to ultra-high (98 mol %) doping level. Inset: Calculated gain efficiencies and corresponding linear fit as a function of GeO_2 core content. (b) Measured Brillouin frequency shift and linewidth versus the GeO_2 core content.

We also measured the experimental Brillouin threshold (P_{th}) at 2-µm wavelength in the two longest optical fiber samples available at 2-µm pumping wavelength, namely, 21 mol % and 75 mol % core doping levels. The simultaneous monitoring of the injected optical power at port 2 of the OC and the backscattered Brillouin signal power at port 3 allowed to draw the power diagram shown in Fig. 3(a). In both cases, we first observe the spontaneous regime of SBS which evolves in a linear way. Then the power of the backscattered Stokes wave strongly increases with injected power. Here we consider 1 % of the injected power to measure the SBS threshold. The HNLF fiber (21 mol %, blue dots) has a Brillouin threshold of 23 dBm, while we measured 26.5 dBm for 75 mol % fiber sample (red dots). A clear difference of 3.5 dB is observed, while the first sample is about 25 times longer than the second one. Note that the second fiber exhibits slightly lower linear losses in the 2-µm waveband (see Table 1 in section 6). In order to compare the opto-acoustic coupling efficiency in those two fibers, we normalize the SBS threshold value with respect to the effective fundamental mode area (A_{eff}) and effective fiber length (L_{eff}) as described previously to compare the elastic wave confinement effects in various photonic crystal fibers [37]. The calculated value for 21-mol % fiber core concentration is then 2.7 W.m.µm^{-2}, while it drops down to 0.54 W.m.µm^{-2} for the 75 mol % doping level (around 5 times lower). This reveals that both strong light and acoustic wave coupling in the second fiber take place through the reduction of fiber core diameter. We can notice that enhancement of both Kerr and Raman have already been reported in such optical fibers [38].

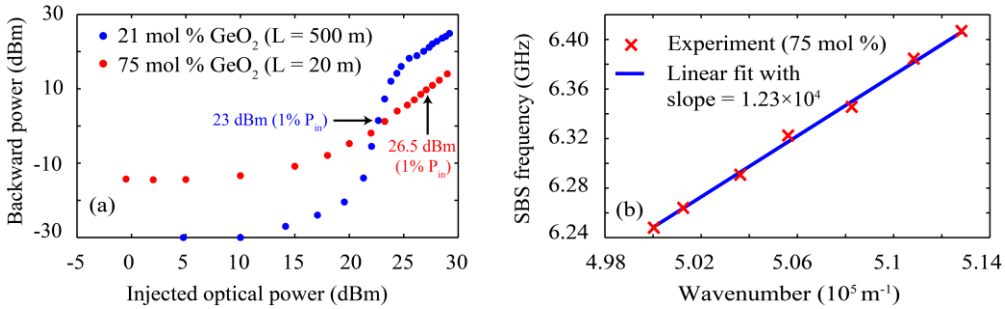

Fig. 3. (a) Experimental measurement of backward Brillouin power as a function of injected power at 2-µm in both fibers with 21 mol % and 75 mol % core GeO_2 content. (b) Measured BFS versus the wavenumber for the fiber with 75 mol % core content. The red line indicates the corresponding linear fit.

Next, we measured the BFS by tuning the pump wavelength around 2-µm for the 75 mol % fiber sample in order to evaluate the elastic velocity. We plotted the Brillouin frequency as a function of the wavenumber ($1/\lambda$), which evolves linearly as it can be observed in Fig. 3 (a). According to the phase matching equation (see Eq. 1 in section 6) that relates the BFS ν_B to the effective refractive index, the elastic velocity and the pump wavelength, the slope of the linear equation allows evaluating the longitudinal velocity v_A, which was found to be 4139 m/s in very good agreement with the previous work at 1.55 µm reported in Ref. [30]. From this measurement and knowing the mass density (ρ = 3270.8 kg.m^{-3}), we can also estimate the elastic tensor constant ($C_{11} = \rho\, {v_A}^2$) of the 75 mol % glass fiber to 56 GPa.

The opto-elastic interaction process in optical fibers can be studied numerically by solving the elastodynamics equation driven by the electrostrictive stress [39,40]. For our germanosilicate glass fibers, we computed the numerical Brillouin spectra based on the theoretical model developed and reported in Ref. [39]. The elastic parameters, such as longitudinal elastic velocity, Young's modulus and mass density, used in our numerical simulation have been previously reported and described in Ref. [30]. Figure 4 depicts the numerical Brillouin spectra at 2-µm wavelength for the five increasing GeO_2-doping levels of our fibers. We confirm numerically that the BFS strongly decreases from 8.4 GHz (SMF-28, black line) up to 6 GHz (98 mol %, purple line) in quite good agreement with our experimental data reported in Fig. 2. Here we underline that all the Brillouin gain spectra exhibit a single elastic resonance, for the frequency detuning considered in the simulation.

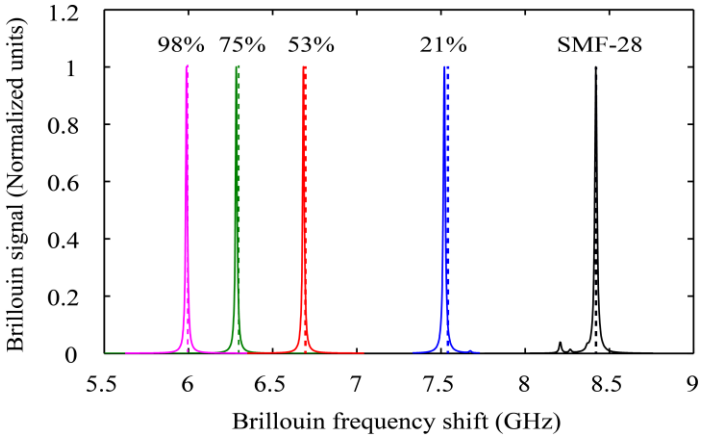

Fig. 4. Numerical simulation of Brillouin gain spectrum at 2-µm wavelength in GeO_2-doped core silica optical fibers (from 3.6 mol % up to 98 mol % doping level). Dashed lines indicate the measured values of BFS in our experiments.

4. Tellurite based optical fiber

A large range of non-silica glasses with broad infrared transmission windows have been successfully drawn into optical fibers so far [41]. Among all of them, the family of tellurium oxides (tellurite) glasses is known to exhibit a higher refractive index (around 2 versus 1.44 for silica glass) as well as a larger Kerr nonlinear index (about 20 times larger than fused silica) and high Raman and Brillouin gain coefficients [42]. Here we present the Brillouin scattering properties measured in a 2-m-long segment of home-made tellurite step-index fiber whose core and cladding compositions are $80TeO_2$-5ZnO-$10Na_2O$-$5ZnF_2$ (TZNF, molar fraction) and $60TeO_2$-5ZnO-$20Na_2O$-$15GeO_2$ (TZNG) respectively [43]. All opto-acoustic parameters of the TeO_2-based optical fiber are listed in Table 1 together with other tested fibers in this article. Figure 5 (a) shows the recorded experimental Brillouin spectrum of the TeO_2-based fiber for

an input power of 15 dBm. The SBS gain spectrum exhibits a main Brillouin frequency peak at 6.165 GHz and a secondary weak peak around 6.145 GHz. Even though our fiber is not strictly single-mode at 2 µm, we carefully checked that this secondary peak cannot be induced by higher-order optical spatial modes (from modal calculations of corresponding effective refractive indices). This peak could be related to the complex compositions of glasses involved in the drawing process of that fiber. By fitting the main peak of the Brillouin gain spectrum with a Lorentzian function (red dashed curve in Fig. 5(a)), we can estimate the Brillouin linewidth to 14.9 MHz. This value is lower than that measured at 1.55 µm wavelength, which is 21 MHz for a Brillouin frequency peak centered at 7.97 GHz. The SBS gain efficiency (g_B/A_{eff}) can be evaluated from the Brillouin gain linewidth and gives the following value of 13 $m^{-1}.W^{-1}$. The theoretical single-pass Brillouin threshold (see Eq. 5 in section 6) is here estimated to be ~1.6 W (32 dBm) for the 2-m-long segment. Due to the specific material compositions used to manufacture our TZN optical fiber, we determined the elastic properties such as longitudinal elastic velocity and Young's modulus by tuning the optical pump wavelength over more than 40 nm around 2 µm to record the linear variation of the BFS (see Fig. 5(b)). According to the phase matching condition of Eq. (1), the longitudinal elastic wave velocity is found to be 3155 m/s, with good similarity with the value reported by Qin et *al*. at 1.54 µm in tellurite-based fibers [21]. Then we can easily estimate the elastic tensor constant (C_{11}) of our tellurite fiber by using the mass density for TZN glass (ρ = 5350 $kg.m^{-3}$) [44], which is found to be 53.3 GPa.

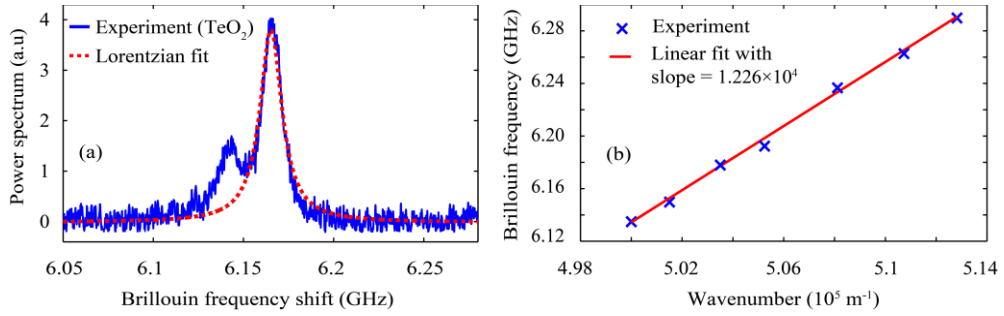

Fig. 5. (a) Experimental backward Brillouin spectrum (blue curve) measured at 2-µm in our TeO_2-based optical fiber and corresponding fit with a Lorentzian function (red dashed curve). (b) BFS versus the wavenumber in order to determine the elastic velocity in our TZN glass. The red line indicates the corresponding linear fit.

5. Chalcogenide glass fiber

Based on the chalcogen chemical elements such as sulfur (S), selenium (Se), and tellurium (Te) combined with many others elements for instance germanium (Ge), arsenic (As), and antimony (Sb), chalcogenide glasses are substantial materials in fiber optic technology, exhibiting both large IR transparency and high Kerr nonlinearity. For instance, the Kerr nonlinear coefficient of these IR glasses is about two-three orders of magnitude larger than standard fused silica glass [41]. These large nonlinearities would allow the development of more compact and low-optical power devices for various applications and make chalcogenide IR glasses as excellent candidates for all-optical processing, Raman amplification, parametric amplification, and supercontinuum generation [41,45]. In our work, we study a 2-m-long segment of chalcogenide step-index fiber whose core and cladding compositions are based on As_2S_3 glass. This optical fiber was manufactured by CorActive from high-purity materials using the double-crucible process [46]. We again used the experimental setup described in Fig. 1 to measure the backward

SBS spectrum. Note that the 2-µm pump was injected into the fiber sample by means of the butt-coupling technique [25,32]. Figure 6 (a) shows the recorded experimental dynamics of the SBS spectrum emerging from the As_2S_3 glass fiber as a function of injected power from 15 to 18 dBm. We clearly observe that the Brillouin spectrum exhibits a multimode signature. Indeed, the chalcogenide fiber is not strictly single-mode at 2 µm, this broad spectrum could be related to the contribution of both higher-order optical modes and the multimode acoustic nature of the As_2S_3 glass fiber. We can interpret the SBS spectrum of Fig. 6(b) as the superposition of one main peak centered at 6.21 GHz and several secondary peaks with distinct amplitudes. Here the Brillouin linewidth was estimated to be 25 MHz for the main peak and then fixed for other peaks, by using a fitting procedure with Lorentzian functions as depicted in Fig. 6(b). Note that Brillouin spectrum was already recorded with a single-mode feature at 1.55 µm with in-house drawn As_2S_3 step-index fibers with smaller core in Ref. [47]. It is worth to mention that similar values of Brillouin frequency shift and linewidth were obtained in a distinct selenium-based chalcogenide suspended-core fiber [32]. Here the SBS gain efficiency can be estimated from the Brillouin gain linewidth to be 45 $m^{-1}.W^{-1}$, which is nearly 180 times larger than that of fused silica glass. We also calculated the single-pass Brillouin threshold, which is here estimated to be 0.37 W (~26 dBm).

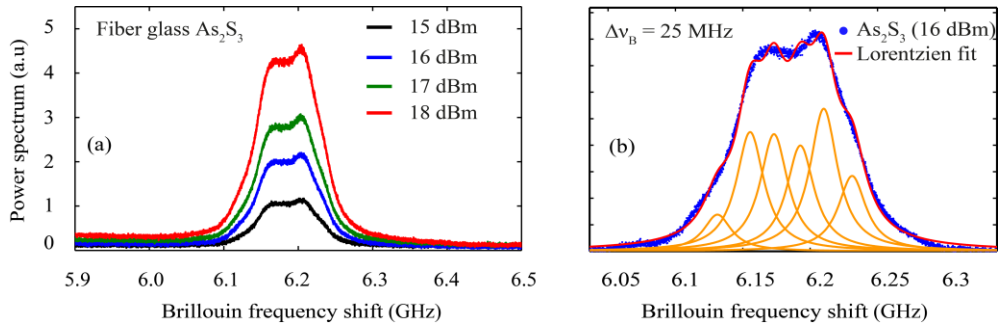

Fig. 6. (a) Experimental backward Brillouin spectra measured at 2-µm wavelength in the As_2S_3 glass step-index fiber as a function of injected pump power (from 15 to 18 dBm). (b) Multiple Lorentzian fit (red and orange curves) of the experimental SBS spectrum (blue dots) recorded at a low pump power (16 dBm).

6. Discussion

Due to the very low SBS efficiency at 2-µm wavelength in the zirconium fluoride-based (ZBLAN) fiber under study (Thorlabs Inc.), we were unable to perform a reliable Brillouin characterization at such a wavelength with the laser source and fiber length available. However, we carried out the study of SBS by pumping at 1.55 µm wavelength. We measured that SBS gain in such fibers is nearly six times lower than in standard silica fiber, thus confirming potential issues of SBS characterization towards 2 µm. Our measurements confirm the previous characterization of SBS in a ZBLAN fiber reported in Ref [48], except the spectral linewidth. Based on this analysis, we can only predict some of the features expected at 2 µm such as the Brillouin frequency shift and linewidth. By using the measured value of acoustic velocity at 1.55 µm, we can then expect that BFS and Brillouin linewidth to be around 6 GHz and 35 MHz when pumping at 2-µm wavelength. Note that the Brillouin linewidth was calculated using the usual product of the quality factor ($Q = \nu_B/\Delta\nu_B$) and the acoustic frequency, which is constant whatever the pump wavelength used.

Overall, the physical information available from direct measurements of the spectrum of Brillouin scattered light is primarily the acoustic velocity from the Brillouin shift and the

acoustic attenuation from the Brillouin linewidth [49,50]. Table 1 summarizes all the experimental results of our study and shows the comparison of both optical and elastic properties between all the fiber samples characterized in this work. Both effective index n_{eff} and effective area A_{eff} of the fundamental optical mode of each fiber are also indicated and based on numerical calculations using a finite element method (COMSOL software) including fiber opto-geometric parameters. It is worth to mention that we simultaneously performed a similar experimental SBS characterization at 1.55 µm wavelength (not shown here for clarity) in all the fiber samples under study. The corresponding results are added in parentheses (blue color) in Table 1. One can then easily compare the SBS efficiency at both wavelengths for all the fibers involved.

Table 1. Comparative analysis of Brillouin and Kerr properties of various glass-based step-index fibers characterized at 2-µm wavelength. Those are a standard silica fiber (SMF-28), four high GeO_2-doped-core fibers, zirconium fluoride-based (ZBLAN), tellurite-based (TZN) and chalcogenide-based (As_2S_3) glass fibers. The specific values at 1.55 µm are given in parentheses (blue color).

Parameters	Units	SMF-28	21 mol %	53 mol %	75 mol %	98 mol %	ZBLAN	TZN	As_2S_3
Core size, Φ	µm	8.2	5	4.7	2.8	2	9	4	6.1
Optical loss, α	dB.m^{-1}	0.022 (2×10^{-4})	0.022 (8×10^{-4})	0.005 (0.01)	0.02 (0.04)	0.1 (0.2)	0.25 (0.125)	0.5 (0.5)	0.2 (0.2)
Length, L	m	500	500	3	20	3	5	2	2
Effective length, L_{eff}	m	180 (494)	181 (477)	2.99 (2.99)	19.1 (18.3)	2.9 (2.8)	4.34 4.66	1.79 (1.79)	1.91 (1.91)
Effective area, A_{eff} *	µm^2	101 (78)	30 (13)	16 (11)	7 (4.7)	5 (3.5)	66 (55)	10 (8)	26 (20)
Effective index, n_{eff} *	-	1.444 (1.446)	1.457 (1.465)	1.481 (1.509)	1.489 (1.519)	1.514 (1.531)	1.475 (1.479)	1.944 (1.960)	2.443 (2.456)
Kerr nonlinear index, n_2 ‡	m^2.W^{-1}	2.44× 10^{-20}	3.10× 10^{-20}	3.75× 10^{-20}	4.38× 10^{-20}	4.97× 10^{-20}	2.93× 10^{-20}	38× 10^{-20}	250× 10^{-20}
Density, ρ ‡	kg.m^{-3}	2210	2507	2960	3271	3598	4350	5350	3200
Photo-elastic constant, p_{12} ‡	-	0.270	0.273	0.280	0.284	0.288	0.196	0.241	0.299
Acoustic velocity, V_a	m.s^{-1}	5960	5059	4480	4139	3898	4040	3155	2600
BFS, ν_B	GHz	8.40 (10.85)	7.55 (9.65)	6.75 (8.72)	6.29 (8.07)	6.00 (7.70)	6.00 † (7.75)	6.17 (7.97)	6.21 (7.96)
SBS linewidth, $\Delta\nu_B$	MHz	15 (28)	35 (55)	65 (89)	73 (94)	76 (98)	35 † (59)	15 (21)	25 (33)
Calculated SBS efficiency g_B/A_{eff}	m^{-1}.W^{-1}	0.25 (0.29)	0.41 (1.0)	0.47 (0.94)	0.99 (2.2)	1.49 (3.0)	0.08 (0.09)	13 (20)	45 (77)
Calculated SBS threshold (10-m segment), P_{th}	W	13 (11)	7.9 (3.0)	7.2 (3.4)	3.3 (1.5)	2.4 (1.3)	55 (40)	0.42 (0.3)	0.09 (0.05)
Calculated FOM (10-m segment)	-	0.10 (0.14)	0.24 (0.29)	0.50 (0.46)	0.63 (0.54)	0.66 (0.61)	0.58 (0.75)	0.30 (0.31)	0.21 (0.21)

* Simulated values † Not able to be measured ‡ From literature

The impact of pumping wavelength, index guiding features and material properties can be retrieved by simply recalling the following fundamental relations that describe BFS in the spectral domain [49–51]:

- the Brillouin frequency shift is $\nu_B = 2n_{eff}v_A/\lambda$ (1)

where v_A is the acoustic velocity in the glass material, and λ the optical pump wavelength.

- the Brillouin gain is $g_B = \frac{2\,\pi\,{n_{eff}}^7\,{p_{12}}^2}{c\,\lambda^2\,\varrho\,v_A\,\Delta\nu_B} = \frac{2\,\pi^2\,{n_{eff}}^7\,{p_{12}}^2\,T_B}{c\,\lambda^2\,\varrho\,v_A} = \frac{2\,\pi^2}{c\,\lambda^2} M\,T_B$ (2)

where c is the velocity of light, p_{12} is the photo-elastic constant of the glass material, ϱ the material density, $\Delta\nu_B$ is the full width at half-maximum of the Brillouin gain spectrum. Spectral width $\Delta\nu_B$ is related to the phonon lifetime $T_B = 1/(\pi\,\Delta\nu_B)$. A figure of merit M is usually introduced to characterize the efficiency of acousto-optic devices as follows:

$$M = \frac{{n_{eff}}^7\,{p_{12}}^2}{\varrho\,v_A} \quad (3)$$

And finally, the photon lifetime can be estimated from direct measurement of the spectral width $\Delta\nu_B$ or from the data of the velocity v_A and attenuation coefficient α_A of acoustic waves as follows:

$$T_B = \frac{1}{\alpha_A\,v_A} \quad (4)$$

In general, acousto-optic devices are developed by choosing acousto-optic media with high figure-of-merit M, which then implies a large refractive index, a large photo-elastic constant and a low acoustic velocity (see Eq. (3)). A well-known example of common material that exhibits these suitable characteristics is the tellurium dioxide (TeO_2) crystal, even associated with a large transmission window. However, such properties are usually associated with high acoustic attenuation [51]. But glass materials still offer large possibilities in selecting their composition by mixing minor molecular constituents to modify the resulting acousto-optic features. In the following, we discuss some of the general physical behaviors, which can be captured from the above relations and data of Table 1.

Firstly, similar trends are reported between the 1.55- and 2-µm wavebands for the Brillouin shift and linewidth of all the fibers, since pumping at longer wavelength decreases the frequency shift (as described by Eq. (1)) as well as the linewidth. The latter can be explained through Eq. (4) by the fact that acoustic losses are known to evolve in a quadratic manner with the Brillouin shift [52], thus increasing the phonon lifetime T_B.

Secondly, our results show that the Brillouin frequency shift of distinct GeO_2-doped silica glass fibers strongly decreases, for instance at 2 µm, from 8.4 GHz to 6 GHz, while the Brillouin gain spectrum width significantly broadens up to 78 MHz for 98-mol % GeO_2 core content. Here we can note that the doping level influences the mass density so that the acoustic velocity is reduced (inversely proportional to the square root of the density [53]), as well as the frequency shift. By contrast the Brillouin linewidth broadens with the GeO_2 core content, since the acoustic losses are here strongly dependent on the index-controlled guiding of acoustic waves unlike in bulk glasses [17]. In particular, the contribution of shear acoustic waves cannot be neglected in such small core fibers, thus leading to Brillouin linewidth broadening [39]. Next, the SBS gain efficiency g_B/A_{eff} in such GeO_2-doped step-index silica fibers significantly increases up to 6 times that of standard silica fiber (0.25 $W^{-1}.m^{-1}$) mainly because of the strong mode confinement in the single-mode regime obtained through the higher refractive index difference between fiber core and cladding.

Thirdly, we explore the Brillouin properties in the main families of infrared-glass fibers commonly used in nonlinear fiber optics, namely zirconium fluoride-based (ZBLAN), tellurite-based (TZN) and chalcogenide (As_2S_3) fibers. It clearly appears that the fluoride fiber exhibit

Brillouin characteristics similar to previous germanosilicate fibers in terms of frequency shift and linewidth (since acoustic velocity and refractive index values are of the same order than for GeO_2-doped-core fibers). By contrast, the Brillouin gain efficiency of the ZBLAN fiber is very weak (even three times lower than in standard silica fiber) and results from a reduced figure of merit M, due to the intrinsic features of the glass material, namely a low photo-elastic constant and a large density. Next, we show that the Brillouin frequency and SBS linewidth of the tellurite glass fiber at 2 µm are around 6.17 GHz and 15 MHz respectively. In that case, the low acoustic velocity induced by the huge density of the TZN fiber is compensated by a high refractive index, so that the frequency shift is comparable with the case of GeO_2-doped-core fibers. However, the Brillouin linewidth is as narrow as the one of the standard silica fiber and a very high effective gain is also measured (very high in comparison with other oxide glasses, 52 times larger than in SMF-28). Such values are definitely attractive from an applicative point of view. The high gain is mainly caused by the higher refractive index [22], whereas the narrow linewidth is reached through a low acoustic velocity and moderate acoustic losses when compared with SMF-28. Finally, the SBS gain spectrum from the chalcogenide (As_2S_3) optical fiber shows a broadband and multi-peak Brillouin spectrum localized around 6.2 GHz when pumping at 2 µm. The SBS efficiency in such fiber is estimated to be ~45 $m^{-1}.W^{-1}$, which is about 180 times larger than in standard silica fiber due to the strong contribution of the high refractive index of chalcogenide glass. Again, the frequency shift is similar to that of the tellurite fiber since the effect of very low acoustic velocity is counteracted in Eq. (1) by a higher refractive index. As predicted by Eq. (4), the Brillouin linewidth is here larger than in the SMF-28 even with a strongly reduced acoustic velocity since acoustic attenuation is known to be significantly larger in chalcogenides [54].

Given that all the fibers were studied with different lengths, we calculated and reported the theoretical single-pass Brillouin threshold (P_{th}) for a unique and practical fiber length of 10 meters in Table 1, based on the following equation [8]:

$$P_{th} = \frac{21 * A_{eff} * K}{g_B L_{eff}} \quad (5)$$

with K = 1.5 and $L_{eff} = (1 - \exp(-\alpha L))/\alpha$: the effective fiber length. The SBS threshold for the fluoride fiber is one order of magnitude higher than for germanosilicate fibers and two/three orders of magnitude higher than for tellurite and chalcogenide fibers. Beyond the SBS efficiency, we can also compare the Kerr efficiency of all glass fibers used in our experiment, we also estimated the following nonlinear figure of merit: FOM = $2\pi\, n_2 P_{th} L_{eff}/(A_{eff}\lambda)$, where n_2 is the Kerr nonlinear index of the glass. This parameter (estimated here for a 10-m-long fiber segment) describes the Kerr nonlinearity efficiency of optical fiber including the SBS-associated pump power limit [19], in particular by providing the maximum nonlinear phase shift available from the nonlinear fiber (without the detrimental Brillouin effect on Kerr processes). For the standard silica glass fiber, the FOM has been calculated to be ~0.1 at 2-µm wavelength, which appears poorly effective compared to the other fibers under study. For instance, the FOM of high GeO_2-doped-core fiber (53 mol %) is about 5 times larger than SMF-28 due to the excellent optical confinement associated to low losses. By comparing to other infrared-glass fibers with high nonlinear index, germanosilicate fibers with high doping levels remain the best solution for Kerr-based nonlinear applications using continuous-wave optical pumping in the 2-µm waveband. Note that such fibers also facilitate the development of all-fiber devices with easy splicing operation to the standard silica fibers.

7. Conclusion

In summary, we investigated the main properties of SBS in various types of infrared step-index optical fibers operating in the 2-µm waveband, as well as at 1.55 µm. Several glass families with good transparency at such wavelengths and their numerous variants in composition offer large possibilities in engineering the resulting acousto-optic features. Even if the SBS phenomenon in step-index optical fibers is mainly driven by the intrinsic material properties, we confirm that the main characteristics of the Brillouin process such as the frequency shift, the spectral linewidth and gain can be also tuned by tailoring the step index in such a simple fiber design.

For instance, the Brillouin frequency shift can be controlled over more than 2 GHz by simply increasing the GeO_2 doping level in the silica fiber core, and that such heavily doped germanium optical fibers can exhibit a large effective Brillouin gain boosted by the tight optical confinement. As expected, the most efficient fibers in terms of effective SBS gain (enhancement factor up to 52 and 180 for the tellurite and chalcogenide fibers compared to SMF-28) are based on acousto-optic media with high figure-of-merit M (i.e. basically with high refractive index), namely tellurite and chalcogenide glasses even if such materials are characterized by stronger acoustic and optical losses. In contrast, the ZBLAN glass fiber presents a much higher power threshold than the SMF28 (i.e., a weak SBS efficiency), it then appears as an excellent candidate for SBS mitigation in high-power applications, fiber amplifiers and telecommunication systems.

This work gives an overview of the SBS features in step-index fibers suitable for the promising 2-µm spectral window, thus paving the way for the design and development of a new class of compact all-fibered Brillouin-based devices for optical processing applications, frequency conversions, widely-tunable narrow-linewidth lasers and sensing [55–58].

8. Funding

Agence Nationale de la Recherche (ANR) (ANR-17-EUR-0002, ANR-15-IDEX-0003, ANR-16-CE24-0010-03). Conseil Régional de Bourgogne-Franche-Comté.

References

1. F. Gunning and B. Corbett, "Time to Open the 2-µm Window?," Opt. Photonics News **30**, 42–47 (2019).
2. D. J. Richardson, "New optical fibres for high-capacity optical communications," Philos. Trans. R. Soc. Math. Phys. Eng. Sci. **374**, 20140441 (2016).
3. W. Cao, D. Hagan, D. J. Thomson, M. Nedeljkovic, C. G. Littlejohns, A. Knights, S.-U. Alam, J. Wang, F. Gardes, W. Zhang, S. Liu, K. Li, M. S. Rouifed, G. Xin, W. Wang, H. Wang, G. T. Reed, and G. Z. Mashanovich, "High-speed silicon modulators for the 2 µm wavelength band," Optica **5**, 1055–1062 (2018).
4. M. Lamy, C. Finot, J. Fatome, M. Brun, P. Labeye, S. Nicolleti, A. Bogris, D. Syvridis, M. A. Ettabib, D. J. Richardson, P. Petropoulos, and K. Hammani, "Ten gigabit per second optical transmissions at 1.98 µm in centimetre-long SiGe waveguides," Electron. Lett. **53**, 1213–1214 (2017).
5. F. C. G. Gunning, N. Kavanagh, E. Russell, R. Sheehan, J. O'Callaghan, and B. Corbett, "Key enabling technologies for optical communications at 2000 nm," Appl. Opt. **57**, E64–E70 (2018).
6. A. Parriaux, K. Hammani, and G. Millot, "Two-micron all-fibered dual-comb spectrometer based on electro-optic modulators and wavelength conversion," Commun. Phys. **1**, 1–7 (2018).
7. M. Lamy, C. Finot, P. Colman, J. Fatome, G. Millot, G. Roelkens, B. kuyken, and K. Hammani, "Silicon Waveguides for High-Speed Optical Transmissions and Parametric Conversion Around 2 µm," IEEE Photonics Technol. Lett. **31**, 165–168 (2019).
8. G. P. Agrawal, *Nonlinear Fiber Optics, 6th ed.* (Academic Press, 2019).
9. E. p. Ippen and R. h. Stolen, "Stimulated Brillouin scattering in optical fibers," Appl. Phys. Lett. **21**, 539–541 (1972).
10. K. O. Hill, B. S. Kawasaki, and D. C. Johnson, "cw Brillouin laser," Appl. Phys. Lett. **28**, 608–609 (1976).
11. K. H. Tow, Y. Léguillon, S. Fresnel, P. Besnard, L. Brilland, D. Méchin, D. Trégoat, J. Troles, and P. Toupin, "Linewidth-narrowing and intensity noise reduction of the 2nd order Stokes component of a low threshold Brillouin laser made of Ge10As22Se68 chalcogenide fiber," Opt. Express **20**, B104–B109 (2012).

12. M. Merklein, B. Stiller, K. Vu, S. J. Madden, and B. J. Eggleton, "A chip-integrated coherent photonic-phononic memory," Nat. Commun. **8**, 574 (2017).
13. S. Norcia, S. Tonda-Goldstein, D. Dolfi, J.-P. Huignard, and R. Frey, "Efficient single-mode Brillouin fiber laser for low-noise optical carrier reduction of microwave signals," Opt. Lett. **28**, 1888–1890 (2003).
14. J. Boschung, L. Thevenaz, and P. A. Robert, "High-accuracy measurement of the linewidth of a Brillouin fibre ring laser," Electron. Lett. **30**, 1488–1489 (1994).
15. S. F. Mafang, "Brillouin Echoes for Advanced Distributed Sensing in Optical Fibres," 201 (2011).
16. M. Niklès, L. Thévenaz, and P. A. Robert, "Simple distributed fiber sensor based on Brillouin gain spectrum analysis," Opt. Lett. **21**, 758–760 (1996).
17. M. Niklès, L. Thévenaz, and P. A. Robert, "Brillouin gain spectrum characterization in single-mode optical fibers," J. Light. Technol. **15**, 1842–1851 (1997).
18. S. Shahi, S. W. Harun, and H. Ahmad, "Multi-wavelength Brillouin fiber laser using a holey fiber and a bismuth-oxide based erbium-doped fiber," Laser Phys. Lett. **6**, 454 (2009).
19. J. H. Lee, T. Tanemura, K. Kikuchi, T. Nagashima, T. Hasegawa, S. Ohara, and N. Sugimoto, "Experimental comparison of a Kerr nonlinearity figure of merit including the stimulated Brillouin scattering threshold for state-of-the-art nonlinear optical fibers," Opt. Lett. **30**, 1698–1700 (2005).
20. G. Qin, A. Mori, and Y. Ohishi, "Brillouin lasing in a single-mode tellurite fiber," Opt. Lett. **32**, 2179–2181 (2007).
21. G. Qin, H. Sotobayashi, M. Tsuchiya, A. Mori, T. Suzuki, and Y. Ohishi, "Stimulated Brillouin scattering in a single-mode tellurite fiber for amplification, lasing, and slow light generation," J. Light. Technol. **26**, 492–498 (2008).
22. K. S. Abedin, "Stimulated Brillouin scattering in single-mode tellurite glass fiber," Opt. Express **14**, 11766–11772 (2006).
23. K. S. Abedin, "Observation of strong stimulated Brillouin scattering in single-mode As2Se3 chalcogenide fiber," Opt. Express **13**, 10266 (2005).
24. C. Fortier, J. Fatome, S. Pitois, F. Smektala, G. Millot, J. Troles, F. Desevedavy, P. Houizot, L. Brilland, and N. Traynor, "Experimental investigation of Brillouin and Raman scattering in a 2SG sulfide glass microstructured chalcogenide fiber," Opt. Express **16**, 9398–9404 (2008).
25. K. H. Tow, Y. Léguillon, P. Besnard, L. Brilland, J. Troles, P. Toupin, D. Méchin, D. Trégoat, and S. Molin, "Relative intensity noise and frequency noise of a compact Brillouin laser made of As38Se62 suspended-core chalcogenide fiber," Opt. Lett. **37**, 1157–1159 (2012).
26. D. K. Sharma and S. M. Tripathi, "Chalcogenide glass microstructured optical fiber as a potential candidate for slow-light generation via stimulated Brillouin scattering," J. Non-Cryst. Solids **542**, 120114 (2020).
27. K. H. Tow, Y. Leguillon, S. Fresnel, P. Besnard, L. Brilland, D. Mechin, P. Toupin, and J. Troles, "Toward More Coherent Sources Using a Microstructured Chalcogenide Brillouin Fiber Laser," IEEE Photonics Technol. Lett. **25**, 238–241 (2013).
28. C. Florea, M. Bashkansky, Z. Dutton, J. Sanghera, P. Pureza, and I. Aggarwal, "Stimulated Brillouin scattering in single-mode As2S3 and As2Se3 chalcogenide fibers," Opt. Express **14**, 12063–12070 (2006).
29. J.-C. Beugnot, R. Ahmad, M. Rochette, V. Laude, H. Maillotte, and T. Sylvestre, "Reduction and control of stimulated Brillouin scattering in polymer-coated chalcogenide optical microwires," Opt. Lett. **39**, 482 (2014).
30. M. Deroh, B. Kibler, H. Maillotte, T. Sylvestre, and J.-C. Beugnot, "Large Brillouin gain in Germania-doped core optical fibers up to a 98 mol% doping level," Opt. Lett. **43**, 4005–4008 (2018).
31. Y. Luo, Y. Tang, J. Yang, Y. Wang, S. Wang, K. Tao, L. Zhan, and J. Xu, "High signal-to-noise ratio, single-frequency 2 μm Brillouin fiber laser," Opt. Lett. **39**, 2626–2628 (2014).
32. K. Hu, I. V. Kabakova, T. F. S. Büttner, S. Lefrancois, D. D. Hudson, S. He, and B. J. Eggleton, "Low-threshold Brillouin laser at 2 μm based on suspended-core chalcogenide fiber," Opt. Lett. **39**, 4651–4654 (2014).
33. T. Yin, B.-M. Mao, Y. Wei, and D. Chen, "Widely wavelength-tunable 2μm Brillouin fiber laser incorporating a highly germania-doped fiber," Appl. Opt. **57**, 6831–6834 (2018).
34. M. Deroh, B. Kibler, A. Lemiere, F. Desevedavy, F. Smektala, H. Maillotte, T. Sylvestre, and J.-C. Beugnot, "2-μm Brillouin laser based on infrared nonlinear glass fibers," Appl. Opt. **58**, 6365–6369 (2019).
35. A. Mishra, A. Mishra, R. Pant, and R. Pant, "Efficient Brillouin lasing and multi-Stokes generation at 2004 nm," OSA Contin. **2**, 2826–2833 (2019).
36. J.-C. Beugnot, T. Sylvestre, D. Alasia, H. Maillotte, V. Laude, A. Monteville, L. Provino, N. Traynor, S. F. Mafang, and L. Thévenaz, "Complete experimental characterization of stimulated Brillouin scattering in photonic crystal fiber," Opt. Express **15**, 15517–15522 (2007).
37. P. Dainese, P. S. J. Russell, N. Joly, J. C. Knight, G. S. Wiederhecker, H. L. Fragnito, V. Laude, and A. Khelif, "Stimulated Brillouin scattering from multi-GHz-guided acoustic phonons in nanostructured photonic crystal fibres," Nat. Phys. **2**, 388–392 (2006).
38. E. M. Dianov, I. A. Bufetov, V. M. Mashinsky, A. V. Shubin, O. I. Medvedkov, A. E. Rakitin, M. A. Mel'kumov, V. F. Khopin, and A. N. Gur'yanov, "Raman fibre lasers based on heavily GeO2-doped fibres," Quantum Electron. **35**, 435 (2005).
39. J.-C. Beugnot and V. Laude, "Electrostriction and guidance of acoustic phonons in optical fibers," Phys. Rev. B **86**, 224304 (2012).

40. V. Laude and J.-C. Beugnot, "Generation of phonons from electrostriction in small-core optical waveguides," AIP Adv. **3**, 042109 (2013).
41. G. Tao, H. Ebendorff-Heidepriem, A. M. Stolyarov, S. Danto, J. V. Badding, Y. Fink, J. Ballato, and A. F. Abouraddy, "Infrared fibers," Adv. Opt. Photonics **7**, 379–458 (2015).
42. V. A. G. Rivera, D. Manzani, and V. A. G. Rivera, *Technological Advances in Tellurite Glasses* (Springer, 2017).
43. C. Strutynski, J. Picot-Clémente, A. Lemiere, P. Froidevaux, F. Désévédavy, G. Gadret, J.-C. Jules, B. Kibler, and F. Smektala, "Fabrication and characterization of step-index tellurite fibers with varying numerical aperture for near- and mid-infrared nonlinear optics," JOSA B **33**, D12–D18 (2016).
44. H. Ebendorff-Heidepriem, K. Kuan, M. R. Oermann, K. Knight, and T. M. Monro, "Extruded tellurite glass and fibers with low OH content for mid-infrared applications," Opt. Mater. Express **2**, 432–442 (2012).
45. A. Lemière, F. Désévédavy, P. Mathey, P. Froidevaux, G. Gadret, J.-C. Jules, C. Aquilina, B. Kibler, P. Béjot, F. Billard, O. Faucher, and F. Smektala, "Mid-infrared supercontinuum generation from 2 to 14 μm in arsenic- and antimony-free chalcogenide glass fibers," JOSA B **36**, A183–A192 (2019).
46. R. Mossadegh, J. S. Sanghera, D. Schaafsma, B. J. Cole, V. Q. Nguyen, R. E. Miklos, and I. D. Aggarwal, "Fabrication of single-mode chalcogenide optical fiber," J. Light. Technol. **16**, 214–217 (1998).
47. C. Florea, M. Bashkansky, J. Sanghera, I. Aggarwal, and Z. Dutton, "Slow-light generation through Brillouin scattering in As2S3 fibers," Opt. Mater. **32**, 358–361 (2009).
48. V. Lambin-Iezzi, S. Loranger, M. Saad, and R. Kashyap, "Stimulated Brillouin scattering in SM ZBLAN fiber," J. Non-Cryst. Solids **359**, 65–68 (2013).
49. J. Schroeder, "Light Scattering of Glass," in *Treatise on Materials Science & Technology*, M. Tomozawa and R. H. Doremus, eds., Glass I: Interaction with Electromagnetic Radiation (Elsevier, 1977), Vol. 12, pp. 157–222.
50. I. L. Fabelinskii, "Spectra of Molecular Scattering of Light," in *Progress in Optics*, E. Wolf, ed. (Elsevier, 1997), Vol. 37, pp. 95–184.
51. N. Uchida and N. Niizeki, "Acoustooptic deflection materials and techniques," Proc. IEEE **61**, 1073–1092 (1973).
52. K. Ogusu, H. Li, and M. Kitao, "Brillouin-gain coefficients of chalcogenide glasses," JOSA B **21**, 1302–1304 (2004).
53. L.-G. Hwa, J. Schroeder, and X.-S. Zhao, "Intrinsic Brillouin linewidths and stimulated Brillouin gain coefficients in glasses studied by inelastic light scattering," JOSA B **6**, 833–839 (1989).
54. T. Sonehara, H. Kaminaga, E. Tatsu, S. Saikan, and S. Ohno, "Frequency-modulated stimulated Brillouin spectroscopy in high-refractive-index glasses," J. Non-Cryst. Solids **354**, 1768–1773 (2008).
55. A. Kobyakov, M. Sauer, and D. Chowdhury, "Stimulated Brillouin scattering in optical fibers," Adv. Opt. Photonics **2**, 1–59 (2010).
56. E. Garmire, "Stimulated Brillouin review: invented 50 years ago and applied today," Int. J. Opt. **2018**, (2018).
57. P. Dragic and J. Ballato, "A Brief Review of Specialty Optical Fibers for Brillouin-Scattering-Based Distributed Sensors," Appl. Sci. **8**, 1996 (2018).
58. M. Deroh, T. Sylvestre, J. Chretien, H. Maillotte, B. Kibler, and J.-C. Beugnot, "Towards athermal Brillouin strain sensing based on heavily germania-doped core optical fibers," APL Photonics **4**, 030801 (2019).